

The role of adsorbate–adsorbate interactions in the rate oscillations in catalytic CO oxidation on Pd (110)

Cite as: J. Chem. Phys. 101, 6717 (1994); <https://doi.org/10.1063/1.468420>

Submitted: 22 February 1994 • Accepted: 30 June 1994 • Published Online: 31 August 1998

N. Hartmann, K. Krischer and R. Imbihl



View Online



Export Citation

ARTICLES YOU MAY BE INTERESTED IN

[Mathematical modeling of kinetic oscillations in the catalytic CO oxidation on Pd\(110\): The subsurface oxygen model](#)

The Journal of Chemical Physics **93**, 811 (1990); <https://doi.org/10.1063/1.459451>

[Oscillatory CO oxidation on Pt\(110\): Modeling of temporal self-organization](#)

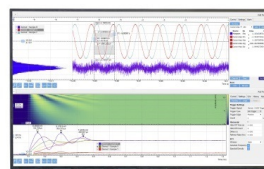
The Journal of Chemical Physics **96**, 9161 (1992); <https://doi.org/10.1063/1.462226>

[A molecular beam investigation of the catalytic oxidation of CO on Pd \(111\)](#)

The Journal of Chemical Physics **69**, 1267 (1978); <https://doi.org/10.1063/1.436666>

Challenge us.

What are your needs for
periodic signal detection?



Zurich
Instruments

The role of adsorbate–adsorbate interactions in the rate oscillations in catalytic CO oxidation on Pd (110)

N. Hartmann, K. Krischer, and R. Imbihl

Fritz-Haber-Institut der Max-Planck-Gesellschaft, Faradayweg 4-6, D-14195 Berlin, Germany

(Received 22 February 1994; accepted 30 June 1994)

The CO+O₂ reaction on Pd(110) exhibits kinetic oscillations above $p_{\text{O}_2} \approx 10^{-3}$ Torr and bistability below this pressure. Based on the reversible formation of subsurface oxygen and the Langmuir Hinshelwood mechanism of catalytic CO oxidation, a mathematical model had been developed which described the occurrence of rate oscillations and most of the qualitative features of the oscillations. This model, however, failed to reproduce the change from bistability to oscillatory behaviour with increasing p_{O_2} . In this paper we demonstrate that by introducing repulsive interactions between CO_{ad} and O_{ad}, the subsurface oxygen model correctly reproduces the experimentally determined stability diagram in $p_{\text{O}_2}, p_{\text{CO}}$ parameter space. The effect of the repulsive interactions is to reduce the activation barrier for penetration of chemisorbed oxygen into the subsurface region, thus facilitating the formation of subsurface oxygen at high coverages. For the improved subsurface oxygen model a bifurcation analysis has been conducted in $p_{\text{O}_2}, p_{\text{CO}}$ parameter space. The influence of the constants in the model has been analyzed likewise with bifurcation theory.

I. INTRODUCTION

The study of oscillatory reactions on single crystal surfaces has led in the past years to the formulation of mathematical models which were successful in reproducing most of the essential qualitative and quantitative features of the experiment.^{1–3} Typically these models simplify strongly the kinetics of the reaction, neglecting for example energetic interactions of the adparticles which are responsible for island formation and lead to coverage dependent kinetic parameters. The reason for the success of such strongly simplified models can be seen in the fact that the behavior of an oscillating system is usually governed by only a few dominating nonlinearities. The coverage dependence of kinetic parameters can, however, not always be neglected and in the following an example is presented that demonstrates how adsorbate–adsorbate interactions can become important in determining the stability diagram of a reaction over a wide parameter space.

The reaction system investigated here is the catalytic CO oxidation on Pd(110) which exhibits rate oscillations at pressures $p > 10^{-3}$ Torr.^{4–12} The existence range of these oscillations has been mapped out in detail between 10^{-3} and 1 Torr by Ehsasi *et al.*^{4,9} Based on the experimental finding that subsurface oxygen formation takes place under oscillatory conditions, a mechanism has been proposed by Ladas *et al.* that explains the rate oscillations by a periodic filling and depletion of the subsurface oxygen reservoir.⁵

The subsurface oxygen mechanism has been cast in a system of three coupled differential equations (DE's) by Bassett *et al.*⁶ This mathematical model explained successfully most of the experimental findings, in particular the reversal of the usual clockwise (cw) rate hysteresis which is observed upon cyclic variation of p_{CO} into a counterclockwise (ccw) hysteresis under conditions where rate oscillations occur.^{5,6} The model, however, failed to reproduce the global bifurca-

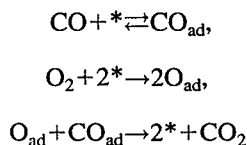
tion diagram in $p_{\text{CO}}, p_{\text{O}_2}$ parameter space, i.e., the change from bistability below $p_{\text{crit}} \approx 10^{-3}$ Torr to oscillatory behavior above p_{crit} . This change is associated with the transition from a true cw hysteresis below p_{crit} to a kinetic ccw hysteresis and rate oscillations above p_{crit} .⁵ The reversal of the rate hysteresis leads to a characteristic cross-shaped bifurcation diagram in $p_{\text{CO}}, p_{\text{O}_2}$ mapped out by Ehsasi *et al.*⁹

Since the original model predicts oscillations at low p_{O_2} and bistability at high p_{O_2} , which is just the opposite of what is observed experimentally, this discrepancy questions the validity of the subsurface oxygen model. As will be shown in this report, the correct bifurcation diagram is obtained if one takes into account the existence of a repulsive interaction between chemisorbed CO and oxygen. This result stresses the importance of adsorbate–adsorbate interactions in surface reactions and it yields further support for the validity of the subsurface oxygen model.

II. THE MODEL

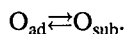
The model used here for Pd(110)/CO+O₂ is essentially identical to the one formulated by Bassett *et al.*, except for some minor simplifications and the introduction of a repulsive interaction between CO_{ad} and O_{ad}. Since a large amount of detailed information about the adsorption and desorption of the reactants and the surface reaction exists in the literature, the initial question has been whether these dependencies should have been put into the model in order to make it more realistic. Such an approach would have made the model very complicated and, moreover, since a number of important parameters are still not known with sufficient accuracy, would have obscured physical insight. For this reason we chose instead to keep the model as simple as possible.

The basis of the model is the Langmuir–Hinshelwood (LH) mechanism of catalytic CO oxidation,



(* denotes a vacant adsorption site)

to which the reversible conversion of chemisorbed oxygen into a subsurface species, O_{sub} , has to be added,



We assume that the reaction is isothermal under low pressure conditions ($p < 1$ Torr) and we first neglect partial pressure variations which arise due to mass balance in the reaction. Furthermore, we restrict the penetration of oxygen into the Pd bulk to the first layer of subsurface sites. We arrive at the following set of equations describing the variation in the CO coverage, θ_{CO} , the oxygen coverage, θ_{O} and in the subsurface oxygen concentration, c , with $0 \leq c \leq 1$;

$$\frac{d\theta_{\text{CO}}}{dt} = k_1 p_{\text{CO}}(1 - \theta_{\text{CO}}) - k_2 \theta_{\text{CO}} - k_3 \theta_{\text{CO}} \theta_{\text{O}}, \quad (1)$$

$$\begin{aligned} \frac{d\theta_{\text{O}}}{dt} &= k_4 p_{\text{O}_2} \exp(-k_5 c) (1 - \theta_{\text{O}} - \theta_{\text{CO}})^2 - k_3 \theta_{\text{CO}} \theta_{\text{O}} \\ &\quad - k_6 \theta_{\text{O}} (1 - c) + k_7 c (1 - \theta_{\text{O}}), \end{aligned} \quad (2)$$

$$\frac{dc}{dt} = k_6 \theta_{\text{O}} (1 - c) - k_7 c (1 - \theta_{\text{O}}), \quad (3)$$

with

$$E_2 = E_2^{\text{O}} - \theta_{\text{CO}} E_{\text{rep}}^{\text{CO,CO}},$$

$$E_6 = E_6^{\text{O}} - \theta_{\text{CO}} E_{\text{rep}}^{\text{CO,O}}.$$

The above equations describe the elementary steps contained in the reaction scheme outlined above; the adsorption (k_1) and desorption (k_2) of CO, the dissociative adsorption of oxygen (k_4), and the surface reaction between adsorbed CO and atomic oxygen to CO_2 (k_3). The diffusion of oxygen from the chemisorbed layer into subsurface sites is treated in the term with k_6 and the diffusion of subsurface oxygen back to the surface layer in the k_7 -term. For simplicity, we do not use the experimentally determined saturation coverages, but let all coverages vary between 0 and 1.

In the formulation of the adsorption steps we neglect precursor kinetics, which experimentally have been found for the adsorption of both gases, CO and oxygen, but assume simple Langmuirian kinetics.^{13,14} We do, however, take into account the observation that preadsorbed oxygen can only to a small extent, block sites for CO chemisorption.¹⁴⁻¹⁷ Therefore the oxygen coverage has been omitted in the adsorption kinetics of CO contained in the term following k_1 in the DE's.

Experimentally it has been shown, both in titration and in steady state experiments, that the reaction between CO and oxygen on Pd(110) proceeds via ordered overlayers of both adsorbates.^{16,17} In the formulation of the model, island

formation has been neglected, since taking these processes into account would lead to complicated functional dependencies.

The feedback between the concentration of subsurface oxygen and the catalytic activity of the surface, which is essential for the oscillation mechanism, is contained in the exponential term with k_5 . This term leads to a very drastic decrease of the oxygen sticking coefficient, s_{O_2} , with increasing subsurface oxygen concentration.^{18,19} In the model, subsurface oxygen thus modulates the catalytic activity via the oxygen adsorption rate.

Between adsorbed particles, attractive or repulsive interactions exist which effectively lead to coverage dependent kinetic parameters. In a rigorous form, these interactions can be treated in lattice gas models, writing the interaction part, H_{int} , of the Hamiltonian as,

$$H_{\text{int}} = \sum_{\text{pairs}} \phi_{ij} c_i c_j + \sum_{\text{triplets}} \phi_{ijk} c_i c_j c_k + \dots,$$

where c_i denotes the occupancy number of lattice site i and ϕ_{ij} , ϕ_{ijk} represent pairwise and triplewise interaction energies, respectively.²⁰ There is, however, little hope of treating successfully a system as complex as the one considered here in such a way. Instead, we use a drastically simplified approach by letting the activation energy, E_i of a process vary linearly with the coverage. We treat the interaction energy as a fit parameter and consider only those terms which are essential for obtaining the desired qualitative changes of the bifurcation diagram. It turned out that in order to reproduce the experimental bifurcation diagram, it was sufficient to make two activation energies, E_2 and E_6 , coverage dependent in the way indicated in the DE's. These constants represent the activation energy for CO desorption and oxygen diffusion into the bulk, respectively.

Both the interaction between CO molecules, $E_{\text{rep}}^{\text{CO,CO}}$, and the interaction between adsorbed CO and adsorbed oxygen, $E_{\text{rep}}^{\text{CO,O}}$, are repulsive. The repulsive interactions between adsorbed CO molecules show up in thermal desorption spectroscopy (TDS) of Pd(110)/CO where they lead to a downward shift in the desorption temperature with increasing coverage, corresponding to a decrease in binding strength.²¹ For the repulsive interaction between CO and oxygen some indirect evidence exists from the observation that coadsorbed CO and oxygen form separate domains on Pd(111) and that the activation energy of the LH reaction decreases with increasing oxygen coverage.^{16,22-24} The existence of a repulsive interaction between CO_{ad} and O_{ad} is consistent with the picture that the strongly electronegative oxygen removes electrons from the conduction band, thus reducing the strength of the backbonding between the metal atoms and CO.

Repulsive interactions between CO and oxygen lower the adsorption strength of adsorbed oxygen and as a consequence the height of the activation barrier for the penetration of chemisorbed oxygen into the Pd bulk becomes smaller at higher coverages. This relationship, which is illustrated by Fig. 1, is equivalent to CO molecules "pushing" the chemisorbed oxygen into subsurface sites. This lowering of the

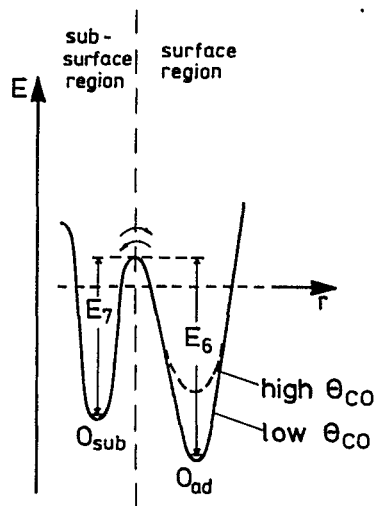


FIG. 1. Schematic energy diagram illustrating the effect of repulsive CO–O interactions on the activation barrier for subsurface oxygen formation. The constants E_6 and E_7 refer to the mathematical model used in the simulations.

activation barrier for the population of subsurface sites is considered to be the main effect of the repulsive interaction between CO_{ad} and O_{ad} . Consequently in the equations we only took this effect into account while we neglected a dependence of the activation energies for the LH reaction and for CO desorption on the combined CO/oxygen coverage. Experimental evidence for the “pushing effect” of the CO–oxygen interaction was obtained in coadsorption studies of hydrogen and CO on Pd(111) and Pd(110).^{25,26} In these studies it was observed that coadsorbed CO forces atomic hydrogen into subsurface sites and accordingly one can expect that a similar effect also exists for subsurface oxygen formation.

Based on the results of TDS and work function measurements of Pd(110)/ O_2 , it has been concluded that the subsurface sites only become populated at coverages above $\theta_{\text{O}}=0.5$, i.e., beyond completion of the $c(2\times 4)\text{-O}$ structure.^{18,19} These results, as well as the formation of a second lower-lying adsorption state in O_2 -TDS at $\theta_{\text{O}}>0.5$, clearly indicate the existence of a repulsive interaction between chemisorbed oxygen atoms. Such an interaction term was initially put into the mathematical model, but was

TABLE II. Temperature independent constants used in the mathematical model.

Description	Constant	Value	References
CO adsorption	k_1	$4.1\times 10^5 \text{ ML s}^{-1} \text{ Torr}^{-1}$	13,14,21
O_2 adsorption	k_4	$7.6\times 10^5 \text{ ML s}^{-1} \text{ Torr}^{-1}$	14
Inhibition of O_2 -adsorption by O_{sub}	k_5	10	fit parameter
Repulsion CO–CO	$E_{\text{rep}}^{\text{CO,CO}}$	2.5 kcal/mol	fit parameter
Repulsion CO–O	$E_{\text{rep}}^{\text{CO,O}}$	5.0 kcal/mol	fit parameter

dropped when the simulations demonstrated that this term was far less important for reproducing the cross-shaped bifurcation diagram than the CO–O repulsion term. Similarly neglected in formulation of the model has been the lowering of the adsorption energy of CO, E_2 , by subsurface oxygen.^{5,17}

The values of the constants which were used in the simulation are summarized in Tables I and II. The constants for CO and oxygen adsorption, k_1 and k_4 , were calculated from kinetic gas theory using the experimentally determined initial sticking coefficients, $S_{\text{CO}}^{\text{O}}=1.0$ and $S_{\text{O}_2}^{\text{O}}=0.86$, for the two gases on Pd(110).^{13,14,21} The activation energy for CO desorption in the limit of zero coverage, $E_2^{\text{O}}=30$ kcal/mol, was obtained from the maximum of the main TDS peak at 480 K with the Redhead formula, assuming $\nu_2=10^{13} \text{ s}^{-1}$.²¹ For the kinetic parameters of the surface reaction, the values of a molecular beam study of CO oxidation on Pd(111) were taken.²⁴ These values were obtained by titrating an oxygen saturated Pd(111) surface with CO in the temperature range $300 \text{ K}\leq T<500 \text{ K}$. Since catalytic CO oxidation on Pd surfaces is considered to be a structure insensitive reaction, such an approach should be valid. In a rather detailed CO titration study of oxygen on Pd(110) at coverages $\theta_{\text{O}}\leq 0.5$, Goschnick *et al.* found different pre-exponentials and activation energies than those of the molecular beam study by Engel and Ertl.¹⁶ Due to the compensation effect the two sets of kinetic parameters yield, however, practically the same values for the reaction rate constant k_3 at 310 K, while at higher temperature the difference in the activation energies starts to lead to substantial differences in k_3 . It turned out that in the simulations a value of k_3 had to be taken which is ten times

TABLE I. Temperature dependent constants used in the mathematical model described in the text. The temperature dependence of the constants is described by an Arrhenius law of the form $k_i=\nu_i \exp(-E_i/RT)$.

Description	Constant	E_i (kcal/mol)	ν_i (s^{-1})	Value at 350 K (ML s^{-1}) ^a	References
CO adsorption	k_2	$30-\theta_{\text{CO}}E_{\text{rep}}^{\text{CO,CO}}$	1×10^{13}	$1.8\times 10^{-6}(\theta_{\text{CO}}=0)$	13,14,21
Surface reaction ^b	k_3	14.0	9.0×10^8	1.6	24
Oxygen diffusion surface–bulk	k_6	$22-\theta_{\text{CO}}E_{\text{rep}}^{\text{CO,O}}$	1.0×10^{10}	$1.8\times 10^{-4}(\theta_{\text{CO}}=0)$	28, estimate
Oxygen diffusion bulk–surface	k_7	20	1.0×10^{10}	3.2×10^{-3}	28, estimate

^aML=monolayer.

^bIn the simulations, a ten times higher value for ν_3 was used, compared to the experimental value given by Ref. 24.

higher than that obtained from the experimental data. This small discrepancy can be explained with simplifications made in the formulation of the model. The applicability of the mathematical model used here to describe the kinetics of catalytic CO oxidation on Pd(110) has been demonstrated by Bondzie *et al.*²⁷ They showed that the results of the titration experiments in Refs. 16 and 17 can be well reproduced with the system of DE's used here.

The kinetics of subsurface oxygen formation had to be approximated, relying on the experimentally determined activation energy of 20 kcal/mol for the bulk diffusion of oxygen as a guideline.²⁸ Using the experimental observation that the time scale of subsurface oxygen segregation is of the order of minutes at 400 K, the frequency factors ν_6 and ν_7 were both fixed at $1.0 \times 10^{10} \text{ s}^{-1}$.⁵ Furthermore a slightly higher value for E_6 than for E_7 was taken, in order to ensure that at lower adsorbate coverages the segregation equilibrium $\text{O}_{\text{ad}} \rightleftharpoons \text{O}_{\text{sub}}$ is on the side of the chemisorbed species. With increasing CO coverage then due to the repulsive CO–O interaction, the equilibrium is shifted towards the subsurface species. This coverage dependent shift in the segregation equilibrium is essential for reproducing the experimental bifurcation diagram.

III. RESULTS

A. Bifurcation diagram in p_{CO} , p_{O_2}

Numerical integration of the system of DE's yields kinetic oscillations of the same type as obtained before with the original model.⁶ Typical examples showing the variation in the reaction rate and in the concentration variables at two temperatures are displayed in Fig. 2. In short, the mechanism for an oscillatory cycle can be described by the following scheme.

In its active state the Pd surface is oxygen covered. As oxygen, however, starts to penetrate into the bulk region, the increase in the subsurface oxygen concentration causes the adsorption rate of oxygen to decrease until a CO covered surface is formed. Since the CO–adlayer inhibits O_2 adsorption, this state of the surface corresponds to a low reaction rate. Now oxygen diffuses back to the surface, where it reacts with CO to form CO_2 . With the depletion of the subsurface oxygen reservoir, the adsorption rate of oxygen starts to rise again, until finally, the CO–adlayer is replaced by an oxygen covered surface and the surface is active again.

The existence range for oscillations has been determined by tracing out the bifurcations of the DE's in p_{CO} , p_{O_2} parameter space. This analysis has been conducted using the continuation algorithms contained in the program package AUTO.²⁹ The resulting bifurcation diagram is displayed in Fig. 3(a). The shaded area in this diagram represents the oscillatory range. The two saddle node (sn) bifurcation lines which mark the boundaries of the bistability range intersect between $p_{\text{O}_2} = 10^{-3} - 10^{-2}$ Torr. Above the intersection kinetic oscillations can occur. The intersection of the bifurcation lines creates a cross which led to the term "cross-shaped" bifurcation diagram. Such a diagram had originally been observed in the experiment as demonstrated by Fig. 3(b).

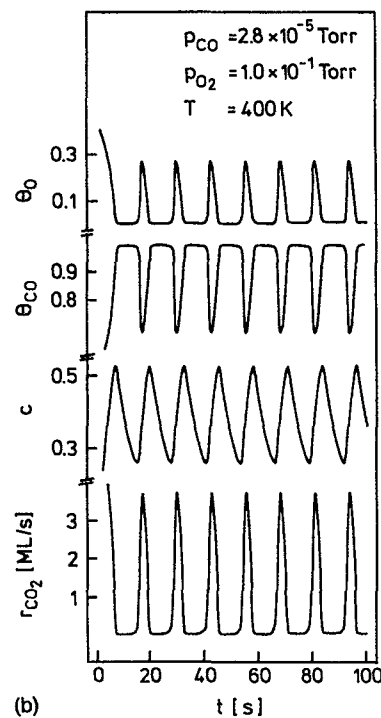
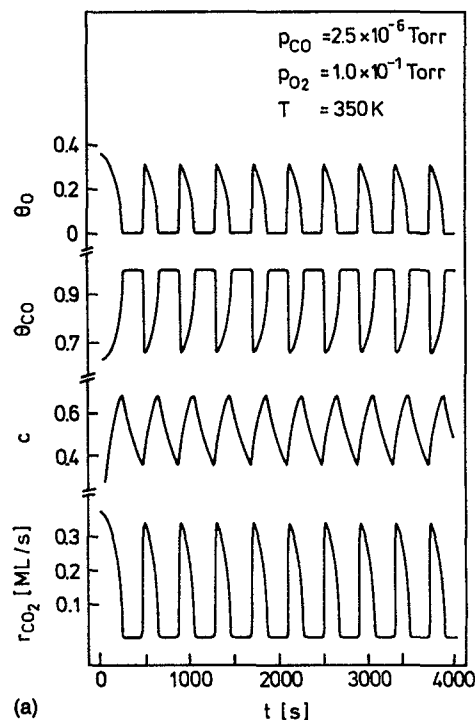
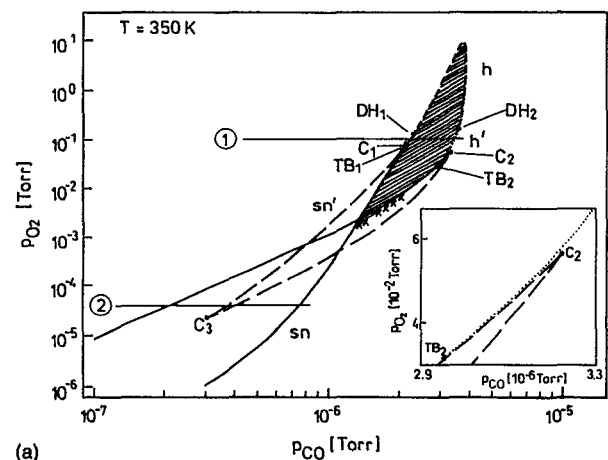
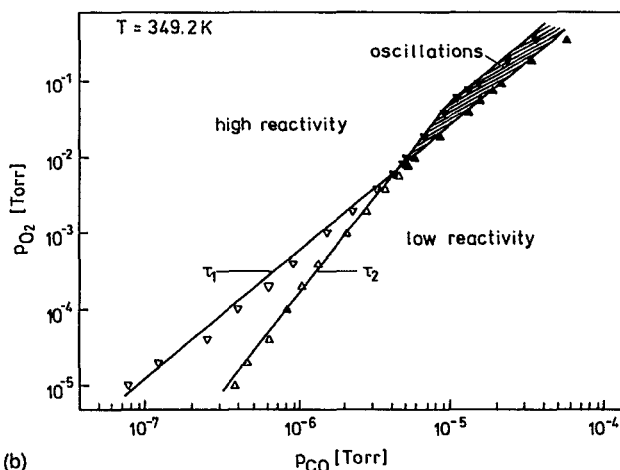


FIG. 2. Simulated rate oscillations demonstrating the influence of the sample temperature on the period of the oscillations. The mathematical model is described in the text and the constants from Tables I and II were taken for the simulation. (a) $T = 350 \text{ K}$; (b) $T = 400 \text{ K}$.

The experimental stability diagram has been mapped out by slowly cycling p_{CO} and plotting the transition points of the resulting rate hysteresis (τ_1, τ_2) in a $p_{\text{CO}}; p_{\text{O}_2}$ diagram.⁹



(a)



(b)

FIG. 3. Cross-shaped bifurcation diagram for catalytic CO oxidation on Pd(110) showing the various regions of monostability, bistability, and oscillatory behavior in p_{CO} , p_{O_2} parameter space at $T=350$ K. (a) Calculated bifurcation diagram in p_{O_2} , p_{CO} parameter space. The shaded area represents the existence range for oscillations. Crosses denote the results of numerical integration. The abbreviations used in the diagram are explained in Table III. The horizontal lines 1 and 2 represent horizontal cuts through the bifurcation diagram shown below in Fig. 4. (b) Experimental bifurcation diagram for catalytic CO oxidation on Pd(110) at $T=349.2$ K, τ_1 and τ_2 represent the boundaries of the bistable region, i.e., the transition points of the rate hysteresis one obtains upon cycling p_{CO} with T and p_{O_2} being kept constant. (After Ref. 9. Reproduced with permission of the authors).

With increasing p_{O_2} , the range of bistability narrows and finally, when the bifurcation lines cross, the cw rate hysteresis turns into a ccw hysteresis. This ccw hysteresis, however, does not represent a true bistability, since when the cycling of p_{CO} is conducted sufficiently slowly or stopped, one observes rate oscillations.

The comparison between the simulated and the experimental bifurcation diagram in Figs. 3(d) and 3(b) demonstrates that, in contrast to the original model, the improved model reproduces all essential qualitative features of the experiment. The range of bistability terminates between 10^{-3} and 10^{-2} Torr and the oscillatory range above the crossing point is of similar width in the simulation and in the experiment. Quantitatively some discrepancy exists with respect to

TABLE III. Abbreviations for the codimension-1 and codimension-2 bifurcations appearing in the present analysis. For codimension-2 also the unfolding of the bifurcation point is given.

Codimension-1		
sn	saddle node	
<i>h</i>	Hopf, supercritical	
<i>h'</i>	Hopf, subcritical	
sl	saddle loop	
sniper	saddle node of infinite period	
snp	saddle node of periodic orbits	
Codimension-2		
<i>C</i>	cusps	sn/sn
TB	Takens–Bogdanov	sn/h/sl
DH	degenerate Hopf	h/snp

the calculated p_{CO} values, which are too low by a factor of 4–10 in equivalent points of the diagrams.

A list of the various abbreviations used in the bifurcation diagram of Fig. 3(a) is given in Table III.³⁰ It should be noted that the plot in Fig. 3(a) only represents a skeleton bifurcation diagram, since the saddle-loop (sl) and saddle node of periodic orbit (snp) bifurcations are not shown. Due to the stiffness of the DE's a continuation of these bifurcations with AUTO turned out to be unreliable; instead the boundaries were complimented by direct integration of the DE's with a fine parameter grid. These calculated boundaries are marked by crosses in the diagram.

The plot in Fig. 3(a) contains three types of codimension-2 points (capital letters) organizing the diagram; cusps (*C*), Takens–Bogdanov (TB) points, and degenerate Hopf (DH) points. The unfoldings of these points are also given in Table III. For a better understanding of the bifurcation diagram two 1D-bifurcation diagrams corresponding to cuts parallel to the x -axis have been constructed. These diagrams are displayed in Fig. 4.

The first cut taken at $p_{O_2} = 4 \times 10^{-5}$ Torr shows the bistability range in a θ_{CO} vs p_{CO} plot given in Fig. 4(a). In addition to the two experimentally observable saddle node (sn) bifurcations (sn_1 and sn_4) one also finds two sn bifurcations associated with unstable branches of the reaction (dashed line). These bifurcations, sn'_2 and sn'_3 have been denoted with a prime in Fig. 4(a) and are represented by dashed lines in Fig. 3(a). In the bistable range one observes two branches of the reaction which are typically seen in catalytic CO oxidation on Pt and Pd surfaces; a high reaction rate branch associated with a low CO coverage and a low reaction rate branch with a dense CO adlayer inhibiting O_2 adsorption.^{1,2} In the reaction rate (not shown here) the diagram of Fig. 4(a) corresponds to a cw hysteresis loop. It should be added that on the low rate branch the CO coverage is close to one in the simulation, while the experimental inhibition coverage for O_2 adsorption is at $\theta_{CO}=0.75$, corresponding to a (4×2) pattern in LEED.¹⁷ This discrepancy is due to the fact that in the DE's an inhibition coverage $\theta_{CO}^{inh}=1$ for O_2 adsorption was used.

The four sn bifurcations terminate in three cusp points denoted by C_1 , C_2 , and C_3 in Fig. 3(a). The relative positions of the sn's and the cusps resemble the unfolding of a

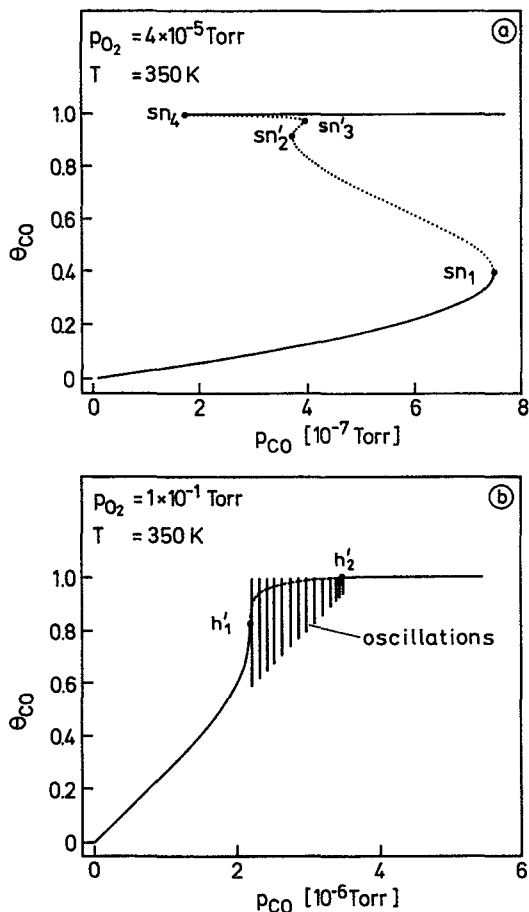


FIG. 4. Horizontal cuts through the bifurcation diagram of Fig. 3(a) illustrating the occurrence of bistability at low p_{O_2} (a) and the development of rate oscillation at high p_{O_2} (b).

so-called butterfly-bifurcation, a situation at which the 5 steady-states coincide.³⁴ Close to the cusp points C_1 and C_2 two Takens–Bogdanov points exist, as can be seen more clearly for C_2/TB_2 in the inset of Fig. 3(a). The dotted line in the inset represents subcritical Hopf bifurcation (h') which emerges from TB_2 . The saddle loop bifurcation, which also emerges from a TB point, is not shown in the figure. At a TB point the saddle node bifurcation changes its character. Hence, between TB_1 and TB_2 (long dashed line in Fig. 3) an unstable node and a saddle is born at the sn bifurcation, whereas on the other side of the TB points (solid line) the sn bifurcation creates a stable node and a saddle point. The two degenerate Hopf (DH) bifurcation points separate the parameter range where the Hopf bifurcation is supercritical from the one where it is subcritical. The Hopf bifurcation is subcritical below DH_1 and DH_2 and supercritical above.

A second cut through the bifurcation diagram showing the subcritical Hopf bifurcations at $p_{O_2} = 10^{-1}$ Torr is displayed in Fig. 4(b). There emerge unstable limit cycles from the subcritical Hopf-bifurcation points which merge with the stable ones in saddle node bifurcations of periodic orbits (snp). As the cut in Fig. 4(b) is close to both degenerate Hopf-bifurcations [DH_1 and DH_2 in Fig. 3(a)] the parameter

ranges in which the stable limit cycles coexist with the unstable ones and the stable steady state (to the left of h'_1 and to the right of h'_2) are very small and in the scale of Fig. 4(b) not discernible. The oscillation amplitude represented by vertical bars has been computed numerically for this diagram. Oscillations occur in the transition range from an active partially CO covered surface, to an inactive completely CO covered Pd(110) surface.

The published experimental data of the rate oscillations show at the high p_{CO} boundary a bifurcation behavior that is consistent with the diagram in Fig. 3(a).⁹ The transition from a subcritical Hopf to a supercritical Hopf with increasing p_{O_2} predicted by the bifurcation diagram, is also seen in the experimental rate oscillations. The amplitude of the rate oscillations grows continuously at $p_{O_2} > 10^{-1}$ Torr, while the data seem to indicate a discontinuous development of the oscillations at $p_{O_2} = 10^{-2}$ Torr. The period of the experimental oscillations does not diverge at the high p_{CO} boundary, as should be the case if a sl or sniper bifurcation were present. At the low p_{CO} boundary of the oscillatory range, the subcritical Hopf predicted by the bifurcation diagram is not seen in the experiment, since the data show a continuous growth of the rate oscillations on this side.

In the formulation of the model we had at first neglected variations in the partial pressure which arise due to mass balance in the reaction and treated the partial pressures as constants. In the experiment, however, only the in-flow rate of the gases is constant, while depending on experimental parameters like chamber volume, pumping rate and surface area of the catalyst, p_{CO} and p_{O_2} will vary, reaching typically oscillation amplitudes of a few percent. We conducted simulations in which we included mass balance in the reaction, using the equation of the continuously stirred tank reactor (CSTR).² The simulations demonstrated that substantial changes in the oscillatory behavior only occur when the p_{CO} variations exceed 5% to 10%. The oscillation frequency then decrease and finally when the amplitude of the p_{CO} variations exceeds 30% a change to bistability is observed.

B. Temperature dependence

In order to illustrate the temperature dependence of the dynamical behaviour of the reaction system, the whole skeleton bifurcation diagram has been calculated for three temperatures, 300, 350, and 400 K. All three diagrams are shown in a single plot in Fig. 5. With increasing temperature the oscillatory range enlarges and becomes shifted towards higher p_{CO} . The bifurcation diagram is quite symmetric with respect to the cross at $T=350$ K, while it becomes strongly asymmetric at $T=300$ and 400 K. In addition the low p_{O_2} limit for oscillations decreases with increasing temperature from 10^{-2} Torr at $T=300$ K to 10^{-4} Torr at $T=400$ K. The temperature range in which kinetic oscillations could be obtained for a fixed $p_{O_2} = 1 \times 10^{-1}$ Torr is shown in a p_{CO} , T -plot in Fig. 6. According to this diagram, rate oscillations should be obtained up to 470 K. Experimentally rate oscillations have only been observed up to ≈ 420 K at $p_{O_2} = 4 \times 10^{-2}$ Torr.^{4,5,9}

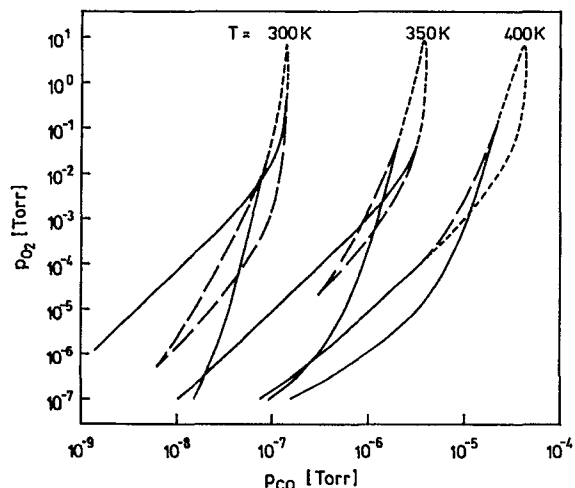


FIG. 5. Skeleton bifurcation diagrams in p_{O_2} , p_{CO} for three different temperatures showing a shift and widening of the existence range for oscillations with increasing temperature.

Despite some drastic simplifications the improved model is capable of reproducing quantitatively, a number of experimental findings which could not be obtained with the original model. This is demonstrated here with the experimental data of the existence range for oscillations in all three parameters, p_{CO} , p_{O_2} , and T . The existence range has been mapped out by Ehsasi *et al.* in the form of "isosteric plots" shown in Fig. 7(a).⁴ The data points in this plot represent the center of the oscillatory range, i.e., they roughly mark the position of the rate maximum upon variation of p_{CO} . The corresponding simulated existence diagram to the experimental data are displayed in Fig. 7(b).

The experimental diagram in Fig. 7(a) exhibits two different slopes associated with different apparent activation energies. The line representing the high- T boundary of the oscillatory range is associated with an activation energy of 22 kcal/mol. The "isosteres" all show the same slope corre-

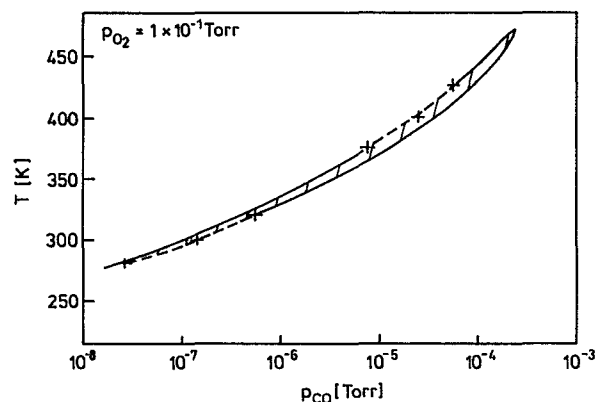
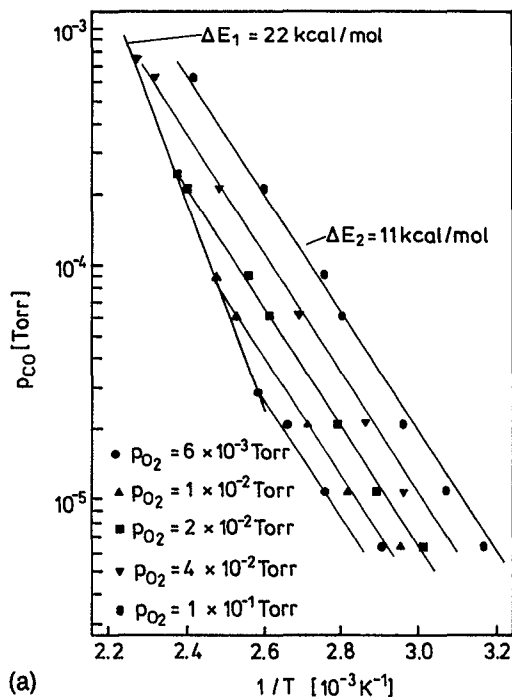
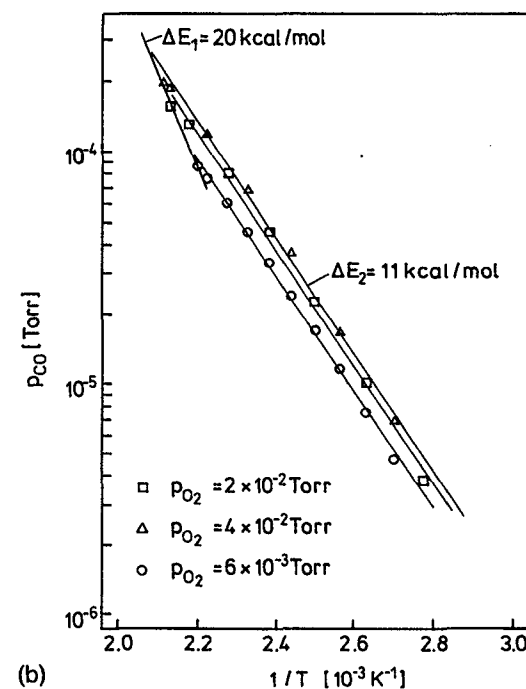


FIG. 6. Existence range for oscillations in p_{CO} , T for fixed $p_{O_2} = 1 \times 10^{-1}$ Torr. The full lines represent a Hopf bifurcation, while the dashed lines with the crosses mark boundaries of a homoclinic bifurcation obtained by numerical integration of the equations.



(a)



(b)

FIG. 7. Existence diagram in p_{CO} , p_{O_2} , T for rate oscillators in the system Pd(110)/CO+O₂. The existence range is mapped out in the form of "isosteric" plots, with each line representing the p_{CO} , T -conditions for rate oscillations at a different p_{O_2} . The data points in this plot represent the center of the existence range for oscillations which in a r_{CO_2} vs p_{CO} plot is given roughly by the position of the rate maximum. (a) Experimental diagram. (After Ref. 4. Reproduced with permission of the authors.) (b) Simulated existence diagram for rate oscillations.

sponding to an activation energy of 11 kcal/mol. These values are very well reproduced by the simulation in Fig. 7(b), since there the "isosteres" have the same slope of 11 kcal/mol, while the slope of the high- T boundary with 20 kcal/

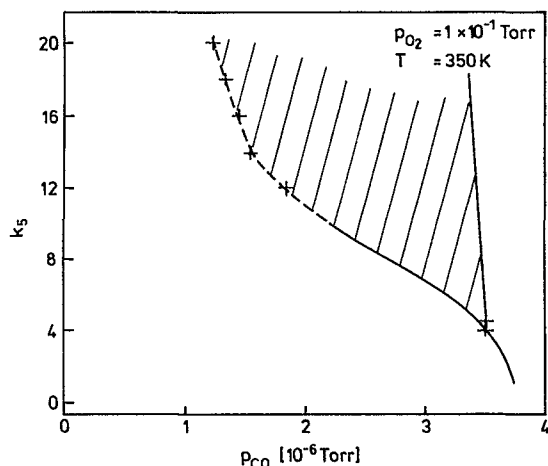


FIG. 8. Bifurcation diagram showing the influence of the inhibition factor for oxygen adsorption, k_5 , on the width of the oscillatory range. The full lines in the diagram represent Hopf bifurcation lines, while the dashed line with the crosses marks a boundary of a homoclinic bifurcation, determined by numerical integration. The shaded region marks the oscillatory range. Below $k_5=4$, the width of the oscillatory range becomes so narrow that it has to be represented by a single line.

mol exhibits only a small deviation from the experimental value. For comparison, the original model without the CO–O interactions, yielded apparent activation energies of 19 and 26 kcal/mol, respectively.⁶ As outlined above some disagreement exists with respect to the calculated p_{CO} values. These are too low by a factor of 5 at $p_{\text{O}_2} = 6 \times 10^{-3}$ Torr and the discrepancy increases with higher p_{O_2} up to a factor of 10 at $p_{\text{O}_2} = 4 \times 10^{-2}$ Torr.

C. Influence of the model parameters

Bifurcation analysis allows one to investigate in a systematic way, the influence of the constants on the behavior of the reaction system by treating them as bifurcation parameters. In this way one can determine which constants play a crucial role in the behavior of a mathematical model. Such an analysis is particularly useful if not all of the constants used in a model can be taken from experiment. In these cases it is especially desirable to have an estimate for the sensitivity of the dynamical system to a particular choice of the corresponding constant. In the following, the influence of the constants which are critical for the behavior of the reaction system are analyzed in the form of 2D-bifurcation diagrams, using p_{CO} and the constant as bifurcation parameters with fixed T and p_{O_2} .

The constant k_5 regulates the inhibitory effect of subsurface oxygen on the oxygen sticking coefficient. Since an exponential dependence has been assumed in the DE's, variations of this constant can have a drastic effect on the reaction system. Figure 8 displays the width of the oscillatory range in p_{CO} when k_5 is varied. This diagram has been constructed partially by continuation of the Hopf bifurcation, and partially by numerical integration. As expected, k_5 has a quite strong influence on the oscillatory behavior of the system. The width of the oscillatory range shrinks practically to zero

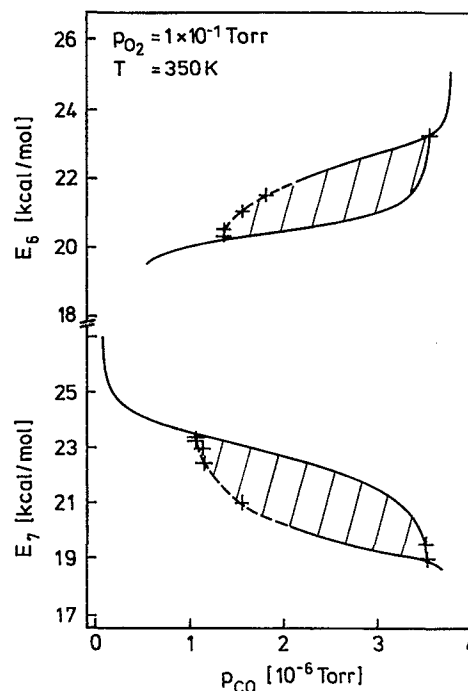


FIG. 9. Bifurcation diagram showing the influence of the activation energies for oxygen diffusion into the bulk, E_6 , and for oxygen segregation to the surface, E_7 , on the width of the oscillatory range. The diagram has been constructed in the same way as Fig. 8.

as k_5 is decreased below ≈ 4.0 . With increasing k_5 , the oscillatory range widens, mainly by shifting the low p_{CO} boundary where the subsurface oxygen concentration is high, while the high p_{CO} boundary with a lower subsurface oxygen concentration remains essentially unchanged. Evidently higher k_5 values lead to an increasingly strong deactivation of the surface and consequently, lower p_{CO} values are required in order to balance a low rate of O_2 adsorption.

The influence of the constants controlling the diffusion of subsurface oxygen on the width of the oscillatory range is shown in Fig. 9. Both the activation energy, E_6 , for penetration of oxygen into the bulk (keeping $E_7 = \text{const}$), and the activation energy, E_7 , for oxygen segregation to the surface (keeping $E_6 = \text{const}$), have been treated as bifurcation parameters and the results are displayed in the same plot. One notes that both parameters can only be varied in a window of ≈ 4 kcal/mol width, above and below which the oscillatory range shrinks practically to zero. This result simply means that oscillations can occur only if a segregation equilibrium between chemisorbed oxygen and subsurface oxygen exists. Otherwise, the surface would remain either in an activated or deactivated state all the time.

Finally, the role of the repulsive CO–O interaction energy, $E_{\text{rep}}^{\text{CO},\text{O}}$, which turned out to be essential for reproducing the cross-shaped bifurcation diagram, has been examined. The resulting diagram in Fig. 10 shows that oscillations are only obtained if $E_{\text{rep}}^{\text{CO},\text{O}}$ lies in a window between 3.8 and 6.6 kcal/mol. Again, for the same reasons already outlined above, the parameter range for $E_{\text{rep}}^{\text{CO},\text{O}}$ is determined by the condition that oxygen diffusion in both directions has to oc-

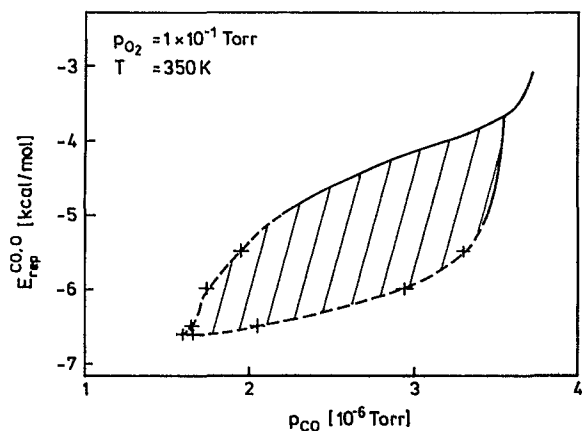


FIG. 10. Bifurcation diagram showing the influence of the parameter $E_{\text{rep}}^{\text{CO},\text{O}}$ which denotes the repulsive interaction between adsorbed CO and oxygen on the width of the oscillatory range. The diagram has been constructed in the same way as Fig. 8.

cur with comparable rates in order to obtain oscillatory behavior.

IV. DISCUSSION

A. Comparison with experiment

The simulations presented here have shown that by taking adsorbate–adsorbate interactions into account, the subsurface oxygen model could reproduce a prominent feature of the Pd(110)/CO+O₂ system, i.e., the cross-shaped bifurcation diagram. Although the model could also reproduce a number of other important features, such as the slopes of the “isosteres” in Fig. 7(a), it is quite evident that a fully quantitative description has not yet been achieved.

The most severe discrepancy between theory and experiment is in the large difference between the period of the simulated and the measured rate oscillations at low temperature ($T=350$ K), which amount to nearly two orders of magnitude. The periods are, however, comparable under conditions of relatively high temperature, at $T>400$ K (see Fig. 2).⁵ If the period of oscillations is determined by the activation barriers of oxygen diffusion then the period of the oscillations should increase strongly with decreasing temperature. This is the case for the simulated oscillations, but the experimental trend is quite the opposite, since the period of the experimental oscillations at $T\approx 350$ K is only of the order of a few seconds.^{4,9}

A reasonable explanation for this discrepancy appears to be that at low temperature and at high pressures the adsorbate coverage on the surface is so large, that repulsive interactions cause a strong lowering of the activation barriers for oxygen diffusion. With respect to the constants used in the model this would mean that, either the value used for the repulsive CO–O interaction was too low, or that the activation barriers for oxygen diffusion into subsurface sites, E_6 and E_7 , are substantially lower than the bulk value of 20 kcal/mol.²⁸ Since there is some evidence from O₂ adsorption experiments on Pd(110) that subsurface sites are already

populated as low as 200 K, the activation barrier for penetration into the bulk appears to be in fact much smaller than the value of 20 kcal/mol determined for bulk diffusion.³³ One can suspect that adsorbate-induced reconstructions of the Pd(110) surface play a very important role in facilitating subsurface oxygen formation, but due to our limited knowledge about these processes, these ideas remain purely speculative (see also the following section).

A shortcoming which is persistent in all the simulations conducted here is that the calculated p_{CO} values are always too low by a factor of 4–10 with respect to the experimental data. The reason for this discrepancy is easily seen in several simplifications built into the model. First, the experimental TDS data show that CO adsorption states are populated at high coverages that have a much smaller adsorption energy than predicted by the coverage dependence of E_2 in the model.²¹ Consequently, in the experiment a higher CO partial pressure will be necessary in order to populate these high coverage states, since a high desorption rate of CO has to be balanced. Second, titration, as well as the steady state experiments, showed that high oxygen coverages reduce the sticking coefficient and the adsorption energy of CO, leading also to an effectively lower adsorption rate of CO than predicted by the model.^{5,17}

As one compares the theoretical predictions with the experiment, one should also be aware that the model using ordinary differential equations (ODE's) describes a spatially homogeneously oscillating surface. Although experiments with a Pd(110) crystal cut into two halves demonstrated that gas-phase coupling synchronizes the oscillations on a large scale,⁷ on a smaller scale in the submillimeter range spatiotemporal patterns are also present. This has been shown in spatially resolved measurements conducted with a photoemission electron microscopy (PEEM).¹⁰ Rate and $\Delta\varphi$ measurements, which average over all or most of the surface area, will therefore exhibit smaller variations than the local concentration variables. At the low p_{CO} boundary of the oscillatory range, the experimental data always showed a gradual growth of the oscillation amplitude, which of course would be inconsistent with the subcritical Hopf bifurcation predicted by the model.⁹ If the surface, however, reacts spatially inhomogeneously, then the continuous growth of the oscillation amplitude might not represent the behavior of the local variables, but be due to an averaging effect. This conclusion, however, needs to be verified in future PEEM experiments.

B. The role of adsorbate–adsorbate interactions

Adsorbate–adsorbate interactions have been investigated quite extensively in the study of ordered overlayers of physisorbed and chemisorbed adparticles.^{20,35} For surface reactions, the influence of adsorbate–adsorbate interactions is usually only discussed in quite general terms, without elaborating a detailed model and without deriving actual values for the magnitude of the interaction energies.^{22,23} The influence of lateral interactions on heterogeneously catalyzed reactions, has been investigated in two Monte Carlo (MC) simulations; one of catalytic CO oxidation³⁶ and one of an oscillating unimolecular decomposition reaction by Vlachos

*et al.*³⁷ Various general schemes for surface reactions have been analyzed by Belyaev *et al.* and by Luss *et al.*, in which coverage dependent activation energies lead to oscillatory solutions.^{38,39} In the modeling of the NO+CO reaction on the unreconstructed Pt(100) surface, a coverage dependent activation energy for desorption had to be introduced in order to obtain kinetic oscillations.⁴⁰

In the reaction system which is considered here, the repulsive CO–O interactions are not essential for the mechanism of the rate oscillations, but they had to be included in order to reproduce the correct bifurcation behavior in p_{O_2} , p_{CO} parameter space, i.e., bistability at low p_{O_2} and oscillatory behavior at high p_{O_2} . The reason why a pressure dependence of the bifurcation behavior arises is easy to see. With rising total pressure, the adsorbate coverages on the surface increase. Consequently, the interactions between adparticles become more and more dominant leading finally to a qualitative change in the dynamical behavior, of the system.

As suggested by recent PEEM experiments of catalytic CO oxidation on Pt(100) and Pt(110), there exists also an alternative mechanism through which high adsorbate coverages can facilitate the formation of subsurface oxygen.^{41,42} In these experiments propagating reaction fronts were found to be followed by a zone of enhanced brightness. The enhanced brightness has been assigned to the formation of a subsurface oxygen species located underneath the topmost layer of metal atoms and therefore associated with a reverse dipole moment.

A mechanism explaining the formation of subsurface oxygen via reaction fronts had already been proposed in earlier experiments, in which the formation of a more tightly bound oxygen species, i.e., of subsurface oxygen, was detected on a Pt(110) surface, which had been faceted during catalytic CO oxidation.⁴³ It was proposed that the $1 \times 1 \rightleftharpoons 1 \times 2$ surface phase transition which is involved in the faceting mechanism, assists the formation of subsurface oxygen. Since the $1 \times 1 \rightleftharpoons 1 \times 2$ phase transition implies the mass transport of 50% of the surface atoms, oxygen atoms will be easily buried underneath the surface layer in the course of the necessary structural rearrangements.

The clean Pd(110) surface does not reconstruct, but as has been demonstrated first by vibrational spectroscopy by King *et al.* and subsequently by field ion microscopy work by Gaussmann *et al.*, high CO coverages ($\theta_{CO} > 0.75$) induce a reconstruction of the 1×2 "missing row" type on the Pd substrate.^{44,45} In addition, it was shown by Dhanak *et al.* that the oxygen superstructures on Pd(110) similarly involve a reconstruction of the substrate.⁴⁶ Although at present there is no direct indication for such a mechanism from PEEM measurements, one can speculate that similar to Pt(100) and Pt(110), structural changes of the substrate play an important role in subsurface oxygen formation on Pd(110). Since the operation of such a mechanism requires the simultaneous presence of large CO and oxygen coverages on Pd(110), the experimental conditions for the formation of the subsurface species should be essentially the same as for the energetic interaction mechanism proposed here, and the only difference would be in the actual microscopic mechanism.

V. CONCLUSIONS

Based on a previous model developed for catalytic CO oxidation on Pd(110), it was shown that the experimentally determined cross-shaped stability diagram can be reproduced by taking repulsive CO–O interactions into account. These interactions lower the activation energy for oxygen diffusion into the bulk, thus facilitating subsurface oxygen formation at higher adsorbate coverages, and hence high p_{CO} , p_{O_2} values. This dependence is considered to be essential for obtaining the experimentally observed change from bistability at lower p_{O_2} , to oscillatory behavior at high p_{O_2} . With the improved model, important experimental facts such as the slopes of the isosteric plots denoting the existence range for oscillations, can be reproduced quantitatively. This result can be considered as further support for the validity of the subsurface oxygen model. Quantitatively a number of discrepancies still exist with respect to the period of the oscillations and the exact determination of the existence range for oscillations in parameter space. These discrepancies have their main origin in the fact that many details of the kinetics of subsurface oxygen formation are still unknown and, quite clearly, more experiments are needed here in order to further improve the model.

ACKNOWLEDGMENTS

The authors thank S. Wasle for the preparation of the drawings. They are indebted to J. H. Block for permission to reproduce Fig. 4 of Ref. 4 and Fig. 4 of Ref. 9.

- ¹G. Ertl, *Adv. Catal.* **37**, 213 (1990).
- ²R. Imbihl, *Prog. Surf. Sci.* **44**, 185 (1993).
- ³F. Schüth, B. E. Henry, and L. D. Schmidt, *Adv. Catal.* **39**, 51 (1993).
- ⁴M. Ehsasi, C. Seidel, H. Ruppender, W. Drachsel, J. H. Block, and K. Christmann, *Surf. Sci.* **210**, L198 (1989).
- ⁵S. Ladas, R. Imbihl, and G. Ertl, *Surf. Sci.* **219**, 88 (1989).
- ⁶M. R. Bassett and R. Imbihl, *J. Chem. Phys.* **93**, 811 (1990).
- ⁷M. Ehsasi, O. Frank, J. H. Block, and K. Christmann, *Chem. Phys. Lett.* **165**, 115 (1990).
- ⁸T. Yamamoto, H. Kasai, and A. Okiji, *J. Phys. Soc. Jpn.* **60**, 982 (1991).
- ⁹M. Ehsasi, M. Berdau, T. Rebitzki, K.-P. Charlé, K. Christmann, and J. H. Block, *J. Chem. Phys.* **98**, 9177 (1993).
- ¹⁰M. Berdau, M. Ehsasi, A. Karpowicz, W. Engel, K. Christmann, and J. H. Block, *Vacuum* **45**, 271 (1994).
- ¹¹I. J. Park and S. I. Woo, *Chem. Phys. Lett.* **212**, 505 (1993).
- ¹²G. G. Yelenin, E. S. Kurkina, and A. G. Makeev (private communication).
- ¹³J. Goschnick, M. Wolf, M. Grunze, W. N. Unertl, J. H. Block, and J. Loboda-Cackovic, *Surf. Sci.* **178**, 831 (1986).
- ¹⁴J. Goschnick, thesis, FU Berlin, 1987.
- ¹⁵J. Goschnick, M. Grunze, J. Loboda-Cackovic, and J. H. Block, *Surf. Sci.* **189/190**, 137 (1987).
- ¹⁶J. Goschnick, J. Loboda-Cackovic, J. H. Block, and M. Grunze, in *Kinetics of Interface Reactions*, Springer Series in Surface Science (Springer, Berlin, 1987).
- ¹⁷S. Ladas, R. Imbihl, and G. Ertl, *Surf. Sci.* **280**, 14 (1993).
- ¹⁸J.-W. He and P. R. Norton, *Surf. Sci.* **204**, 26 (1988).
- ¹⁹J.-W. He, U. Memmert, and P. R. Norton, *J. Chem. Phys.* **90**, 5088 (1989).
- ²⁰K. Binder, *J. Comput. Phys.* **59**, 1 (1981).
- ²¹J.-W. He, *J. Chem. Phys.* **89**, 1170 (1988).
- ²²H. Conrad, G. Ertl, and J. Küppers, *Surf. Sci.* **76**, 323 (1978).
- ²³T. Engel and G. Ertl, *Adv. Catal.* **28**, 1 (1979).
- ²⁴T. Engel and G. Ertl, *J. Chem. Phys.* **69**, 1267 (1978).
- ²⁵H. Conrad, G. Ertl, and E. E. Latta, *J. Catal.* **35**, 363 (1974).
- ²⁶M. P. Kiskinova and G. M. Bliznakov, *Surf. Sci.* **123**, 61 (1982).

- ²⁷V. Bondzie, P. Kleban, and D. A. Browne, *J. Vac. Sci. Technol. A* **11**, 1946 (1993).
- ²⁸J. W. Park and C. J. Altstetter, *Scr. Metall.* **14**, 1481 (1985).
- ²⁹E. Doedel, AUTO, a program for the automatic bifurcation analysis of autonomous systems. *Congress Numerantium* **30**, 265 (1981).
- ³⁰For an introduction to bifurcation analysis, see, for example, Refs. 31 and 32.
- ³¹M. Kubicek and M. Marek, *Computational Methods in Bifurcation Theory and Dissipative Structures* (Springer, New York, 1983).
- ³²R. Seydel, *From Equilibrium to Chaos-Practical Bifurcation and Stability Analysis* (Elsevier, New York, 1988).
- ³³M. Milun, P. Pervan, M. Vajic, and K. Wandelt, *Surf. Sci.* **211/212**, 887 (1989).
- ³⁴P. T. Saunders, *An Introduction to Catastrophe Theory* (Cambridge University, Cambridge, 1980).
- ³⁵(a) L. D. Roelofs and P. J. Estrup, *Surf. Sci.* **125**, 51 (1983); (b) A. Zangwill, *Physics at Surfaces* (Cambridge University, Cambridge, 1988).
- ³⁶H. P. Kaukonen and R. M. Nieminen, *J. Chem. Phys.* **91**, 4380 (1989).
- ³⁷D. G. Vlachos, I. D. Schmidt, and R. Aris, *J. Chem. Phys.* **93**, 8306 (1990).
- ³⁸I. D. Belyaev, M. M. Slinko, U. F. Timoshenko, and M. G. Slinko, *Kinet. Catal.* **14**, 810 (1973).
- ³⁹C. A. Pikios and D. Luss, *Chem. Eng. Sci.* **32**, 191 (1977).
- ⁴⁰R. Imbihl, T. Fink, and K. Krischer, *J. Chem. Phys.* **96**, 6236 (1992).
- ⁴¹H. H. Rotermund, J. Lauterbach, and G. Haas, *Appl. Phys. A* **57** (1993).
- ⁴²J. Lauterbach, G. Haas, H. H. Rotermund, and G. Ertl, *Surf. Sci.* **294**, 116 (1993).
- ⁴³R. Imbihl, M. Sander, and G. Ertl, *Surf. Sci.* **204**, L701 (1988).
- ⁴⁴R. Raval, S. Haq, M. A. Harrison, G. Blyholder, and D. A. King, *Chem. Phys. Lett.* **187**, 391 (1990).
- ⁴⁵A. Gaussmann and N. Kruse, *Catal. Lett.* **1**, 305 (1991).
- ⁴⁶V. R. Dhanak, G. Cornelli, G. Paolucci, K. C. Prince, and R. Rosei, *Surf. Sci.* **260**, L24 (1992).